1

Hydrogen Bonding in Polymeric Materials

1.1 Introduction

Hydrogen-bonding, dipole–dipole, and ionic interactions in polymers have been of great interest to fundamental polymer science, and also industrially, for over 30 years. These secondary or noncovalent interactions can be introduced specifically into polymeric materials to form supramolecular materials displaying interesting thermal, mechanical, surface, and optoelectronic properties. The concept of noncovalent bonding has changed the thinking of polymer scientists, who had been focused for many years primarily on the effects of covalent interactions.

Hydrogen bonds (H-bonds) are interactions that result from dipole–dipole forces between strongly electronegative atoms (e.g., fluorine (F), nitrogen (N), oxygen (O)), and hydrogen atoms; they affect the physical properties and microstructures of many materials [1–6]. For example, water is recognized to form tetrahedral clusters comprising 14 molecules of H_2O; the unusual properties of water arise mainly from the fact that water molecules readily form H-bonds—4 of them—per water molecule, in a tetrahedral geometry [7]. Other famous examples are the H-bonds found in biological systems [8], where they play important roles affecting the three-dimensional structures of nucleic bases and proteins. The DNA double helix is formed from multiple H-bonding interactions between complementary cytosine/guanine (C/G) and adenine/thymine (A/T) base pairs; these noncovalent interactions link the two complementary strands and enable replication. Furthermore, H-bonds greatly influence the secondary structures of polypeptides: the α-helix conformation is stabilized by intramolecular (or intrachain) H-bonding, while the β-sheet conformation is stabilized by intermolecular (or interchain) H-bonding [9, 10]. In addition to these famous natural examples, H-bonding also has several profound effects in unnatural polymeric materials, influencing various physical, thermal, and mechanical properties, including melting points (T_m), crystalline structures, glass transition temperatures (T_g), surface properties, optoelectronic properties, and solubilities (in solvents) and miscibilities (in polymer blends).

Although there are already several reviews on H-bonded polymer blends, copolymers, self-assembled supramolecular structures, and nanocomposite systems [11–21], this book aims to provide a thorough discussion of how H-bonding interactions have been used in research into polymer blends, surface properties,

Hydrogen Bonding in Polymer Materials, First Edition. Shiao-Wei Kuo.

self-assembled block copolymers, mesoporous materials, biomacromolecules, and polyhedral oligomeric silsesquioxanes (POSS) nanocomposites.

1.1.1 Hydrogen Bonds

Hydrogen bonding is a fundamental interaction in chemistry, physics, and biology and has been described extensively in many books [22] and reviews [23]. The H-bond is a directed, attractive, noncovalent bonding interaction between an A–H unit (proton donor) and a B atom (proton acceptor) in the same molecule or in different molecules, where the A and B atoms are generally highly electronegative (e.g., F, N, O), although even C–H groups can be involved in H-bonding and some π-electrons can act as weak H-bond acceptors [24, 25]. The H-bond can also be characterized by its effect on the physical properties or molecular characteristics of a material. A covalent bond usually has strength on the order of 50 kcal mol^{-1}; H-bonds most often have stabilities in the range 1–40 kcal mol^{-1} (in comparison, van der Waals attraction is favorable by only approximately 0.2 kcal mol^{-1}). A strong H-bond has strength in the range 10–40 kcal mol^{-1}; a moderate H-bond, 4–10 kcal mol^{-1}; and a weak H-bond, 1–4 kcal mol^{-1} [26].

Hydrogen bonding can be either an intermolecular or intramolecular phenomenon. An intermolecular H-bond (Figure 1.1) is one for which the donor and acceptor units are found in two different molecules; for an intramolecular H-bond (Figure 1.2) they are in the same molecule. Intermolecular H-bonds are usually linear or near linear, whereas intramolecular H-bonds usually feature some degree of bending. In polymers, two different types of H-bonding can occur for the same functional group, namely, interchain and intrachain H-bonding interactions. For example, the α-helix conformation of a polypeptide is stabilized by intrachain H-bonding, while the β-sheet conformation is stabilized by interchain H-bonding. The strength of an H-bond is strongly dependent on the solvent polarity; the addition of a polar solvent can decrease the H-bond

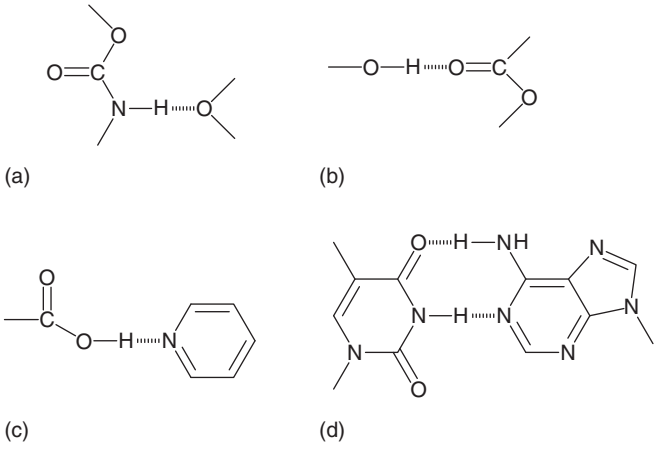

Figure 1.1 Intermolecular H-bonding between two molecules. (a) Urethane–ether complex; (b) hydroxyl–carbonyl complex; (c) acid–pyridine complex; and (d) adenine–thymine complex.

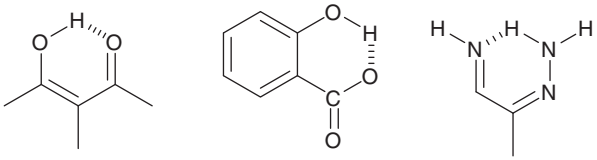

Figure 1.2 Intramolecular H-bonding of a single molecule. (a) Malonaldehyde; (b) salicyclic acid; and (c) formazan.

strength significantly, over several orders of magnitude, because the solvent molecule can also take part in H-bonding interactions. As a result, nonpolar solvents (e.g., toluene, $CHCl_3$, and linear and cyclic alkanes) are mostly used for the preparation of H-bonded supramolecular materials.

1.1.2 Characterization of Hydrogen Bonding

Several spectroscopic methods are commonly used to characterize H-bonds: (i) Fourier transform infrared (FTIR) and Raman spectroscopy, in which the stretching and bending vibrations of the donor or acceptor functional groups are influenced by the presence of H-bonds; (ii) ultraviolet (UV) and fluorescence spectroscopy, which reveal changes in the electronic levels of molecules experiencing H-bond interactions; (iii) nuclear magnetic resonance (NMR) spectroscopy, where changes in chemical shifts can arise from H-bond interactions of the donor and acceptor functional groups; and (iv) X-ray photoelectron (XPS) spectroscopy, where a new shoulder or even a new peak can appear as a result of a change in the chemical environment of an atom perturbed by the H-bonding [27–30].

Among these methods for characterizing H-bonds, by far the most inexpensive and sensitive is FTIR spectroscopy. For example, Figure 1.3 presents the CO stretching range of the FTIR spectra of H-bonded phenolic/PCL blends of various compositions. The signal for C=O stretching in this phenolic/PCL blend splits into two bands: a signal at higher wavenumber (1734 cm^{-1}) corresponding to the free C=O groups of PCL, and one at relatively lower wavenumber (1708 cm^{-1}) representing the C=O groups of PCL H-bonded with phenolic OH groups. If we can resolve these peaks into two Gaussian functions, we can quantify the fraction of H-bonded C=O groups using the appropriate absorptivity ratio between the two peaks. Using this approach, we can see that the fraction of H-bonded C=O groups of PCL increased upon increasing the content of phenolic in the blend [31].

In addition to one-dimensional (1D) infrared (IR) spectra (e.g., in Figure 1.3), two-dimensional (2D) correlation spectroscopy can also be used to characterize H-bonding interactions in polymer materials [32–34]. Through measurements of spectral perturbations in response to temperature, time, composition, or pressure, we can identify inter- or intramolecular H-bond interactions through analyses of the selected bands based on the corresponding 1D infrared spectra. Figure 1.4 displays a typical 2D-IR correlation spectrum of PVPh/PVPK blends in the region 1500–1700 cm^{-1} [35]. The spectrum features two independent axes

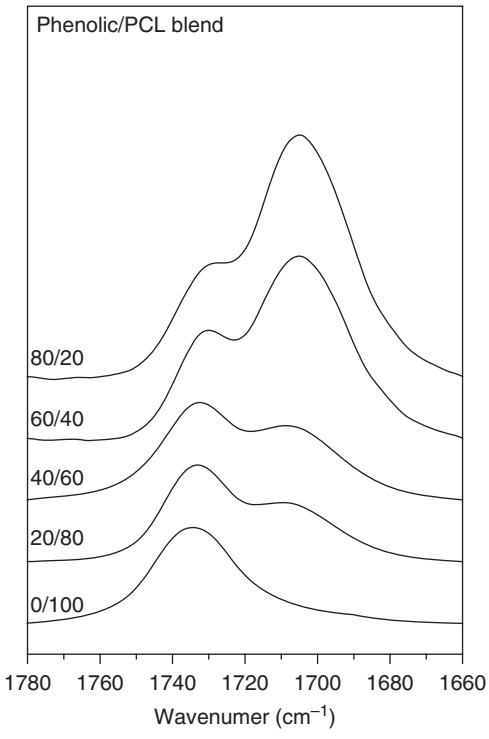

Figure 1.3 Typical infrared (IR) spectra, displaying the C=O stretching region, of phenolic/PCL blends.

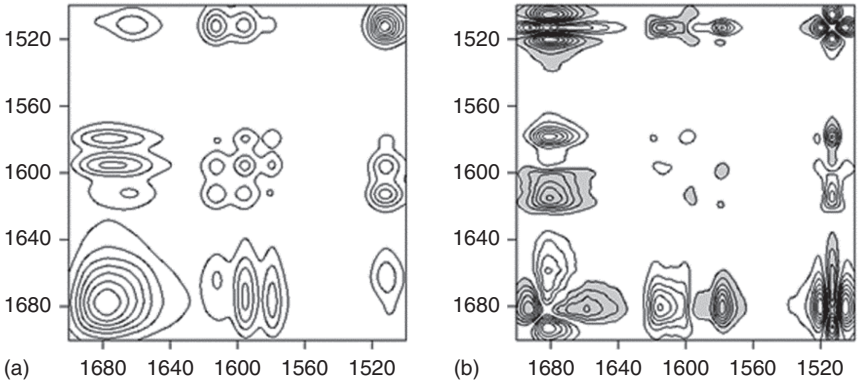

Figure 1.4 2D Fourier transform infrared (FTIR) correlation maps of PVPh/PVPK blends: (a) synchronous and (b) asynchronous maps [35].

for the wavenumber, as well as the correlation intensity. White and shadowed areas represent positive and negative cross-peaks, respectively, in the 2D contour maps. Two types of 2D correlation spectra are generally obtained: synchronous spectra (Figure 1.4a), in which the correlation intensity indicates the relative in-phase degree, and asynchronous spectra (Figure 1.4b), in which the correlation intensity indicates the relative out-of-phase degree. The correlation map in the 2D synchronous spectrum in Figure 1.4a was symmetrical corresponding

to the diagonal line. These intensities of auto-peaks in 2D synchronous spectra should be positive when located at the diagonal line, corresponding to the autocorrelation degree from perturbation-induced molecular vibration. The cross-peaks in 2D synchronous spectra may possess positive (white) or negative (shadow) intensities, corresponding to simultaneous and coincidental changes in the variations of the correlation intensities measured at off-diagonal positions for two different wavenumbers (ν_1, ν_2). A positive cross-peak results when the changes in the signals at these two wavenumbers (ν_1, ν_2) occur in the same direction under the environmental perturbation (i.e., both increase or both decrease). If the signals at the two wavenumbers (ν_1, ν_2) change in opposite directions under the environmental perturbation (i.e., one decreases while the other increases), a negative cross-peak will appear. The asynchronous cross-peaks can also be either positive or negative, giving sequential order information for the external variable. Figure 1.4b displays the asymmetric 2D asynchronous spectrum corresponding to the diagonal line.

Figure 1.4a reveals positive cross-peaks for the correlation intensity of the signal at 1680 cm^{-1} with those at 1612 and 1510 cm^{-1}, implying intermolecular H-bonding between the phenolic OH groups of PVPh (1612 and 1510 cm^{-1}) and the C=O groups of PVPK (1680 cm^{-1}), with changes in the same direction. It also reveals positive cross-peaks between the signals at 1612 cm^{-1} (PVPh) and 1580 cm^{-1} (PVPK), implying π–π interactions among the aromatic rings of PVPh and PVPK, again in the same direction. As a result, the intermolecular interactions in PVPh/PVPK blends arise not only from intermolecular OH···O=C H-bonding but also from π–π interactions of the aromatic rings. Figure 1.4b displays the 2D asynchronous spectrum of the PVPh/PVPK blend. The positive peaks at (1580, 1612 cm^{-1}), (1612, 1680 cm^{-1}), and (1680, 1580 cm^{-1}) imply that the sequence of order in the spectra is 1612 > 1680 > 1580 cm^{-1}, based on the changes in intensity of these three observed bands according to Noda's rule [36].

Solid-state NMR spectroscopy can also provide useful information for identifying H-bonding, by observing the line shapes or chemical shifts in the spectra that are sensitive to the local chemical environment. Figure 1.5 provides an example of this chemical shift in the ^{13}C solid-state NMR spectra of a phenolic/PVAc binary blend [37]. Downfield chemical shifts occurred for the signals of the C=O groups of PVAc (by about 3 ppm) and the OH-substituted carbon atoms in the phenolic resin (by about 2.3 ppm), implying that the H-bonding interactions existed in the phenolic/PVAc blend. The chemical environments of neighboring nuclei can also be influenced by H-bonding in polymer blend systems, leading to downfield chemical shifts that are widely used to provide evidence for H-bonding in polymer blend systems. In addition, the C=O units in the ^{13}C solid-state NMR spectra were also resolved into two peaks—similar to the situation in FTIR spectra (cf. Figure 1.3)—that represented the free (high field at about 171 ppm) and H-bonded (downfield at about 174 ppm) C=O groups of PVAc. The fraction of H-bonded C=O groups of PVAc increased upon increasing the concentration of phenolic resin, similar to the observation in the FTIR spectroscopic analysis. Solid-state NMR spectroscopy can also provide evidence for the miscibility scale of H-bonded polymer blend systems, determined from the proton spin–lattice relaxation time [T_1(H)] [38–40]; a single, composition-dependent value of T_1(H)

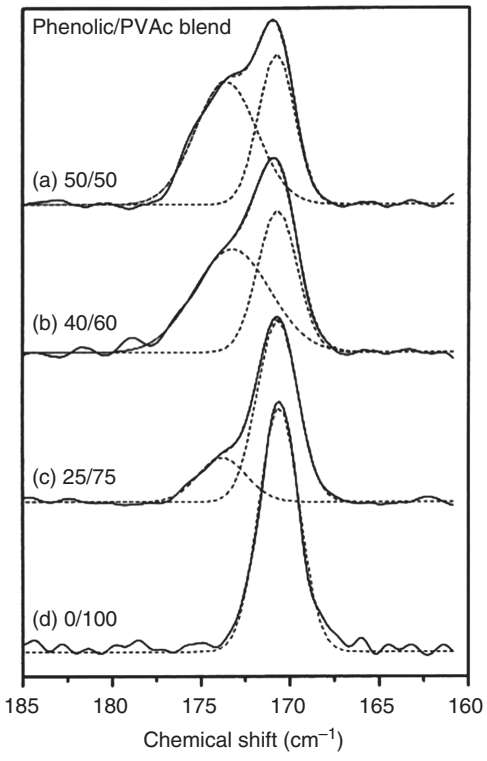

Figure 1.5 Solid-state nuclear magnetic resonance (NMR) spectra and corresponding curve-fitting results for phenolic/PVAc blends [37].

in a polymer blend system represents a homogeneous amorphous phase to the scale by the spin diffusion within the time occurring.

References

1 Errera, J. and Mollet, P. (1936) Intermolecular forces and O—H absorption bands in alcohols at 3. *Nature*, **138**, 882.

2 Etter, M.C. (1990) Encoding and decoding hydrogen-bond patterns of organic compounds. *Acc. Chem. Res.*, **23**, 120–126.

3 Schwager, F., Marand, E., and Davis, R.M. (1996) Determination of self-association equilibrium constants of ethanol by FTIR spectroscopy. *J. Phys. Chem.*, **100**, 19268–19272.

4 Bereo, M., Ikeshoji, T., Liew, C.C., Terakura, K., and Parinello, M. (2004) Hydrogen bond driven chemical reactions: Beckmann rearrangement of cyclo-hexanone xxime into ε-caprolactam in supercritical water. *J. Am. Chem. Soc.*, **126**, 6280–6286.

5 Parmar, D., Sugiono, E., Raja, S., and Rueping, M. (2014) Complete field guide to asymmetric BINOL-phosphate derived Brønsted acid and metalcatalysis: History and classification by mode of activation; Brønsted acidity, hydrogen bonding, ion pairing, and metal phosphates. *Chem. Rev.*, **114**, 9047–9153.

6 Jones, W.D. (2000) Conquering the carbon–hydrogen bond. *Science*, **287**, 1942–1943.

7 Fecko, C.J., Eaves, J.D., Loparo, J.J., Tokmakoff, A., and Geissler, P.L. (2003) Ultrafast hydrogen-bond dynamics in the infrared spectroscopy of water. *Science*, **301**, 1698–1702.

8 Watson, F.P. and Crick, F.H. (1953) Genetical implications of the structure of deoxyribonucleic acid. *Nature*, **171**, 964–967.

9 Pauling, L., Corey, R.B., and Branson, H.R. (1951) The structure of proteins: two hydrogen-bonded helical configurations of the polypeptide chain. *Proc. Natl. Acad. Sci. U.S.A.*, **37**, 205–211.

10 Pauling, L. and Corey, R.B. (1951) Configurations of polypeptide chains with favored orientations around single bonds two new pleated sheets. *Proc. Natl. Acad. Sci. U.S.A.*, **37**, 729–740.

11 Coleman, M.M. and Painter, P.C. (1995) Hydrogen bonded polymer blends. *Prog. Polym. Sci.*, **20**, 1–59.

12 Jiang, M., Mei, L., Xiang, M., and Zhou, H. (1999) Interpolymer complexation and miscibility enhancement by hydrogen bonding. *Adv. Polym. Sci.*, **146**, 121–196.

13 He, Y., Zhu, B., and Inoue, Y. (2004) Hydrogen bonds in polymer blends. *Prog. Polym. Sci.*, **29**, 1021–1051.

14 Binder, W.H. and Zirbs, R. (2007) Supramolecular polymers and networks with hydrogen bonds in the main-and side-chain. *Adv. Polym. Sci.*, **207**, 1–78.

15 Bouteiller, L. (2007) Assembly via hydrogen bonds of low molar mass compounds into supramolecular polymers. *Adv. Polym. Sci.*, **207**, 79–112.

16 ten Brinke, G., Ruokolaine, J., and Ikkala, O. (2007) Supramolecular materials based on hydrogen-bonded polymers. *Adv. Polym. Sci.*, **207**, 113–178.

17 Xu, H., Srivastave, S., and Rotello, V.M. (2007) Nanocomposites based on hydrogen bonds. *Adv. Polym. Sci.*, **207**, 179–198.

18 Kuo, S.W. (2008) Hydrogen-bonding in polymer blends. *J. Polym. Res.*, **15**, 459–486.

19 Fox, J.D. and Rowan, S.J. (2009) Supramolecular polymerizations and main-chain supramolecular polymers. *Macromolecules*, **42**, 6823–6835.

20 Huang, S.H., Chiang, Y.W., and Hong, J.L. (2015) Luminescent polymers and blends with hydrogen bond interactions. *Polym. Chem.*, **6**, 497–508.

21 Voorhaar, L. and Hoogenboom, R. (2016) Supramolecular polymer networks: hydrogels and bulk materials. *Chem. Soc. Rev.*, **45**, 4013–4031.

22 Jeffrey, G.A. and Saenger, W. (1991) *Hydrogen Bonding in Biological Structures*, Springer, Berlin, Heidelberg, New York.

23 Calhorda, M.J. (2000) Weak hydrogen bonds: theoretical studies. *Chem. Commun.*, 801–809.

24 Kuo, S.W., Huang, W.J., Huang, C.F., Chan, S.C., and Chang, F.C. (2004) Miscibility, specific interactions, and spherulite growth rates of binary poly (acetoxystyrene)/poly (ethylene oxide) blends. *Macromolecules*, **37**, 4164–4173.

25 Kuo, S.W., Huang, C.F., Tung, P.H., Huang, W., Huagn, J., Chang, J.M., and Chang, F. (2005) Synthesis, thermal properties, and specific interactions of

high T_g increase in poly (2,6-dimethyl-1,4-phenylene oxide)-block-polystyrene copolymers. *Polymer*, **46**, 9348–9361.
26 Grabowski, S.J. (2004) Hydrogen bonding strength—measures based on geometric and topological parameters. *J. Phys. Org. Chem.*, **17**, 18–31.
27 Skrovanek, D.J., Howe, S.E., Painter, P.C., and Coleman, M.M. (1985) Hydrogen bonding in polymers: infrared temperature studies of an amorphous polyamide. *Macromolecules*, **18**, 1676–1683.
28 Wang, L., Wang, Z., Zhang, X., Shen, J., Chi, L., and Fuchs, H. (1997) A new approach for the fabrication of an alternating multilayer film of poly(4-vinylpyridine) and poly(acrylic acid) based on hydrogen bonding. *Macromol. Rapid Commun.*, **18**, 509–514.
29 Chu, P.P. and Wu, H.D. (2000) Solid state NMR studies of hydrogen bonding network formation of novolac type phenolic resin and poly(ethylene oxide) blend. *Polymer*, **41**, 101–109.
30 Jiao, H., Goh, S.H., and Valiyaveettil, S. (2001) Mesomorphic interpolymer complexes and blends based on poly(4-vinylpyridine)–dodecylbenzenesulfonic acid complex and poly(acrylic acid) or poly(*p*-vinylphenol). *Macromolecules*, **34**, 7162–7165.
31 Kuo, S.W. and Chang, F.C. (2001) The study of miscibility and hydrogen bonding in blends of phenolics with poly (ε-caprolactone). *Macromol. Chem. Phys.*, **202**, 3112–3119.
32 Noda, I. (1989) Two-dimensional infrared spectroscopy. *J. Am. Chem. Soc.*, **111**, 8116–8118.
33 Noda, I. (2006) Progress in two-dimensional (2D) correlation spectroscopy. *J. Mol. Struct.*, **799**, 2–15.
34 Sun, B., Lin, Y., Wu, P., and Siesler, H.W. (2008) A FTIR and 2D-IR spectroscopic study on the microdynamics phase separation mechanism of the poly (*N*-isopropylacrylamide) aqueous solution. *Macromolecules*, **41**, 1512–1520.
35 Kuo, S.W. (2008) Effect of copolymer compositions on the miscibility behavior and specific interactions of poly (styrene-*co*-vinyl phenol)/poly (vinyl phenyl ketone) blends. *Polymer*, **49**, 4420–4426.
36 Noda, I. and Ozaki, Y. (2004) *Two-Dimensional Correlation Spectroscopy: Applications in Vibrational and Optical Spectroscopy*, John Wiley & Sons, Ltd, Chichester.
37 Huang, M.W., Kuo, S.W., Wu, H.D., Chang, F.C., and Fang, S.Y. (2002) Miscibility and hydrogen bonding in blends of poly (vinyl acetate) with phenolic resin. *Polymer*, **43**, 2479–2487.
38 Caravatti, P., Neuenschwander, P., and Ernst, R.R. (1986) Charcterization of polymer blends by selective proton spin-diffusion NMR measurements. *Macromolecules*, **19**, 1889–1895.
39 Wang, J., Cheung, M.K., and Mi, Y. (2001) Miscibility in blends of poly (4-vinylpyridine)/poly (4-vinylphenol) as studied by ^{13}C solid-state NMR. *Polymer*, **42**, 3087–3093.
40 Wang, J., Cheung, M.K., and Mi, Y. (2002) Miscibility and morphology in crystalline/amorphous blends of poly(caprolactone)/poly(4-vinylphenol) as studied by DSC, FTIR, and ^{13}C solid state NMR. *Polymer*, **43**, 1357–1364.